Journal of Materials Chemistry A

Accepted Manuscript

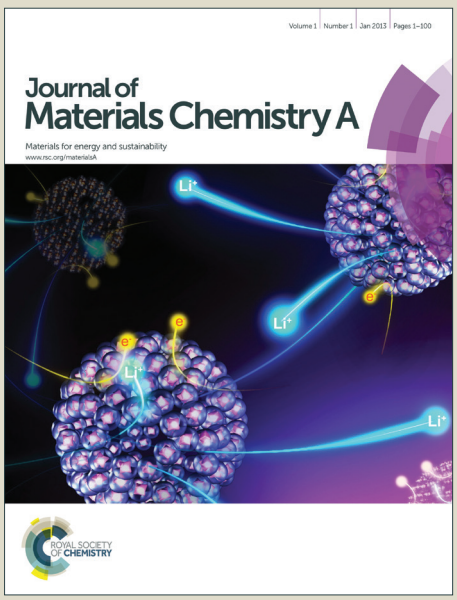

ROYAL SOCIETY OF CHEMISTRY

www.rsc.org/materialsA

Cite this: DOI: 10.1039/c0xx00000x

www.rsc.org/xxxxxx

COMMUNICATION

A Robust Hydrogen Evolution Catalyst Based on Crystalline Nickel Phosphide Nanoflakes on Three-Dimensional Graphene/Nickel Foam: High Performance for Electrocatalytic Hydrogen Production from pH 0-14

Ali Han, Song Jin, Huanlin Chen, Hengxing Ji, Zijun Sun, Pingwu Du*

Received (in XXX, XXX) Xth XXXXXXXXX 20XX, Accepted Xth XXXXXXXXX 20XX
DOI: 10.1039/b000000x

Design and preparation of highly active catalysts for hydrogen evolution reaction (HER) is very important for water splitting. Herein, we report a highly active HER catalyst, which is synthesized by loading nanostructured nickel phosphide (Ni_2P) on three-dimensional few-layer graphene/nickel foam (G@NF). G@NF was successfully prepared by a chemical vapor deposition process in the presence of methane at high temperature. Compared with nickel phosphide, G@NF, as well as commercial platinum, the Ni_2P-G@NF catalyst exhibited very high activity in electrocatalytic H_2 production from water (~7 mV overpotential in alkaline solutions, pH ~14; and ~30 mV overpotential in acidic solution, pH ~0). The high catalytic activity of Ni_2P-G@NF is attributed to the excellent performance of Ni_2P, the large 3D framework which facilitates proton accessibility and electron transfer, and the high surface area.

The hydrogen evolution reaction (HER) is a reductive half-reaction of water splitting and possesses technological significance in that it enables the production of hydrogen, a clean and alternative energy carrier with great potential.[1-5] Catalysts play very important roles in achieving highly efficient HER.[6-9] A recent review has discussed both theoretical and experimental studies of HER electrocatalysts mainly focusing on the electronic structure, surface (electro)chemistry, and molecular design.[10] Platinum is a well-known active catalyst for HER and it has been used to enable remarkable performance for hydrogen production.[1,5] Unfortunately, platinum's rarity and high cost limit its widespread application.[6,11] MoS_2,[12] WS_2,[13] and their analogs (such as MoB[14] and Mo_2C[15]) are active noble-metal-free HER catalysts used as alternatives to Pt, but they often perform well only in acidic conditions. Compared with Mo and W-based HER catalysts, the first-row transition metals are much more abundant, they have been also studied as electrocatalysts for HER. For example, Ni-based HER catalysts include alloys of Ni-Mo,[16-18] Ni-Mo-Zn,[19] and Ni dendrites[20] et al. However, these Ni-based catalysts are not stable in strong acid, so the problem still remains of finding acid- and base-tolerant HER catalysts that can perform feasibly in proton exchange membrane-based electrolyzer. By using a nitrogen-doping approach, the stability of Ni-Mo alloys is improved but their HER activity has not been significantly improved compared to the noble metals such as Pt.[21] CoS has been studied as an effective HER catalyst, while it shows low activity under alkaline conditions and it is not very stable in strong acid.[22] Yang, Vojislav and coworkers reported a 3D bimetallic $PtNi_3$ nanoframes, which exhibited surprisingly high activity of HER, as well as high activity for oxygen reduction reaction (ORR).[23]

Recently, Lewis, Schaak, and coworkers developed nanostructured nickel phosphide (Ni_2P) for efficient HER catalysis (Tafel plot, slope = 41 mV/dec) with good acid-tolerant properties.[24] A later report demonstrated the highly active activities of hollow and multifaceted Ni_2P nanoparticles for HER in both acidic and basic solutions.[25] More recently, Sun and coworkers developed a high-performance, acid-stable hydrogen evolution cathode composed of CoP nanomaterials on carbon fiber cloth (CoP/CC).[26] The onset potential of CoP/CC for HER is as low as 38 mV with a low slope for the Tafel plot (51 mV/dec).

In this present study, we report a simple method to synthesize a binder-free 3D Ni_2P/few-layer graphene/nickel foam (Ni_2P-G@NF) cathode by anchoring Ni_2P nanoflakes over 3D graphene/nickel foam and investigate its catalytic HER properties. The growth of graphene layers on nickel foam (NF) can protect it from being oxidized in air and simultaneously afford good electrical contact from deposited active catalyst to the current collector.[27] Thus, such structure can enhance the interfacial electron transfer and improve the catalytic activity. Compared with Ni_2P and conventional platinum, 3D Ni_2P-G@NF cathode exhibits extraordinarily high activity for HER from pH 0-14.

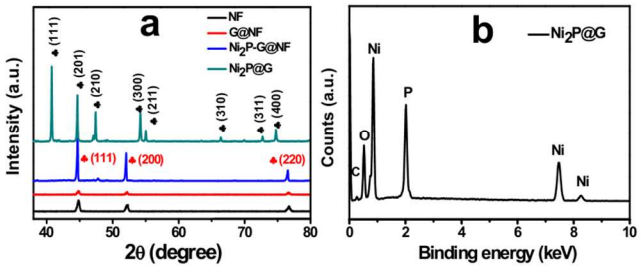

Figure 1. a) X-ray diffraction patterns of the as-prepared 3D NF (black), G@NF (red), Ni_2P-G@NF (blue) and Ni_2P@G electrodes (green). The black and red symbols represent the diffraction peaks of Ni_2P and metallic Ni, respectively; b) EDX spectrum of the as-prepared 3D Ni_2P@G.

The 3D electrode hybridizing graphene layers with nickel foam (G@NF) was fabricated *via* a chemical vapor deposition (CVD) method according to the reported literature.[27-28] After coating with graphene, the amount of the nickel element on the surface was significantly reduced (Figure S1, EDX spectra). The subsequent coating of Ni_2P on G@NF to make Ni_2P-G@NF cathode was successfully accomplished by sprinkling a thick layer of red phosphorous over the G@NF, which was annealed at 750 ºC under argon for 1 hour with a heating rate of 10 ºC/min. Since the metallic nickel is not stable in strong acid, we therefore fabricated 3D Ni_2P@G electrode with no nickel support for the HER test in acidic solution. Ni_2P@G was prepared by dissolving the nickel from Ni_2P-G@NF in 6 M HCl at 80 ºC for 5 hours, followed by washing with deionized water.

Figure 1a shows the X-ray diffraction (XRD) patterns of the NF, G@NF, Ni_2P@G, and Ni_2P-G@NF electrodes. The patterns show eight diffraction peaks for Ni_2P@G at 2θ = 40.74, 44.77, 47.32, 54.04, 55.10, 66.31, 72.59 and 74.54, which can be assigned to the (111), (201), (210), (300), (211), (310), (311), and (400) planes of hexagonal Ni_2P (PDF#:74-1385, Figure S2), respectively. Other diffraction peaks from NF such as metallic Ni can also be detected at 2θ = 44.62, 52.10, and 76.64, corresponding to (111), (200), and (220) planes of cubic Ni (PDF#:01-1260). However, no carbon diffraction peak was observed in the XRD patterns which was probably due to the relatively weak diffraction peaks of the carbon. The EDX spectrum of Ni_2P@G (Figure 1b) indicates that the electrode was made of Ni and P with an atom ratio of ~2:1. The results indicate Ni_2P was successfully grown over the G@NF electrode.

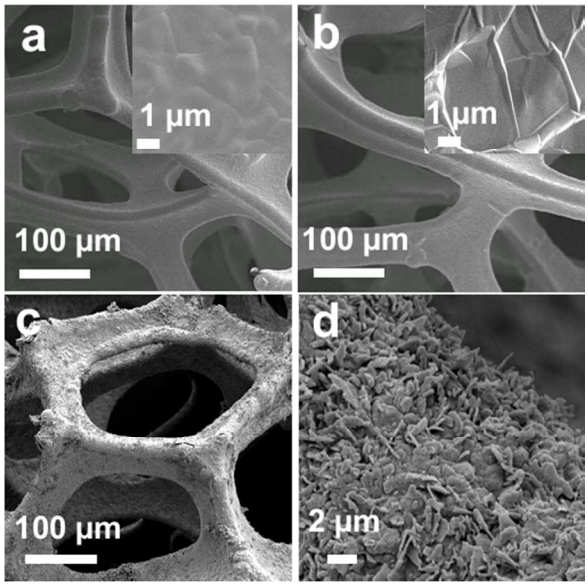

Figure 2. a) SEM images for the nickel foam (NF). The insert picture is the high magnified image of NF; b) SEM images for the graphene layers/nickel foam (G@NF). The insert picture is the high magnified image of G@NF; c and d) SEM images of the as-prepared 3D Ni_2P-G@NF. Figure d is the high magnified image of Ni_2P-G@NF.

The growth of graphene layers and Ni_2P over the nickel foam was further studied by scanning electron microscope (SEM). Figure 2a shows that the nickel foam has a 3D cross-linked network structure with numerous macropores. A high-magnification SEM image (Figure 2a, inset) indicates that the surface of the nickel foam is clean with no wrinkles. It can be seen that the nickel foam still remains its 3D cross-linked networks after a CVD process for the growth of graphene layers (Figure 2b). The high-magnification SEM image shows that thin layers of graphene with some ripples and wrinkles are readily grown on nickel foam surface (Figure 2b, inset).

After deposition of Ni_2P, the surface morphology of the electrode changes significantly. Figures 2c and 2d show the SEM images of the Ni_2P nanostructure on the 3D cross-linked G@NF surface. The surface of the Ni_2P-G@NF electrode becomes quite rough because of the formation of Ni_2P on the surface. The high-magnification SEM image demonstrates that Ni_2P nanoflakes are vertically packed on G@NF, forming a 3D porous surface morphology (Figure 2d). The thickness of the nanoflakes was close to 180-220 nm, as seen in Figure S3. Moreover, after removing the nickel foam template by acid treatment, the SEM image shows that Ni_2P@G still retains a 3D interconnected network structure without any signs of collapse (Figure S4). Figure S5 shows the XPS spectra of the Ni_2P-G@NF electrode. The Ni_2P spectrum consists of several components, in which the peaks at 852.8 eV and 857.0 eV corresponds to Ni (0) in G@NF and $Ni^{\delta+}$ in Ni_2P,[20] respectively, suggesting the presence of Ni elements in different chemical states (Figure S5a). In the P $2p_{3/2}$ spectrum (Figure S5b), the peak at 129.5 eV is attributed to the binding energy for $P^{\delta-}$ in Ni_2P.[15,26] The appreciable peak of P $2p_{3/2}$ at 134.6 eV was probably because of the oxidation of phosphorous into phosphates, upon exposure of the Ni_2P nanoflakes to air for long time. Similar observations have been also reported in the literature.[29-30]

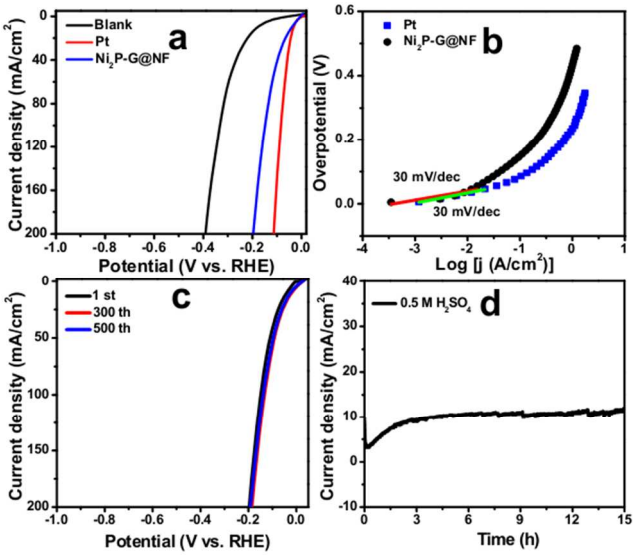

Figure 3. a) Polarization curves of Ni_2P-G@NF electrode in 0.5 M H_2SO_4 (pH = 0) with a scan rate of 5 mV s^{-1}, along with G@NF and a Pt electrode for comparison; b) The Tafel plot for Ni_2P-G@NF electrode and the Pt electrode; c) Polarization data for the Ni_2P-G@NF electrode in 0.5 M H_2SO_4 initially and after 300, 500 CV sweeps; d) Time-dependent current density for Ni_2P-G@NF electrode under overpotential of 55 mV for 15 h.

Figure 3a shows the linear sweep voltammetry (LSV) curve of the Ni_2P-G@NF electrode in 0.5 M H_2SO_4 (pH ~0) with an Ag/AgCl electrode as the reference electrode. A significant catalytic curve was observed for catalytic HER. Considerable catalytic current (1.0 mA/cm^2) was obtained under an

overpotential of as low as 30 mV, demonstrating highly efficient performance of Ni_2P-G@NF cathode for hydrogen production. This value is comparable to recent reports using noble-metal-free CoP electrocatalyst,[26,31] and Ni_2P electrocatalyst.[24-25] For comparison, a Pt electrode (d = 0.3 cm) was used as the working electrode to perform the same experiment. To achieve the catalytic current density at 10 mA/cm^2, the Ni_2P-G@NF cathode requires 55 mV overpotential and Pt only needs 6 mV, as seen from Figure 3. The Tafel plots in Figure 3b show that the slope for the Pt electrode is ~30 mV/dec, which is consistent with the value reported in the literature.[24] The Ni_2P-G@NF electrode exhibits a slope of ~30 mV/dec from 0 to 40 mV, which is close to that of the Pt electrode. It demonstrated that the recombination reaction (Tafel reaction) is the rate limiting step.[32] At higher overpotentials (η = 60-140 mV), the Tafel slope was increased to ~107 mV/decade. These values do not match well with the expected Tafel slopes of 29, 38, and 116 mV/decade, each of which correlate with a different rate-determining step of the HER.[33] The low overpotential and small slope of the Tafel plot for HER indicate the present Ni_2P-G@NF cathode is among the best noble-metal-free HER catalysts, including Mo-based HER catalysts,[34-35] CoP,[26,31] and Ni_2P,[24] as seen in Table S1. The Faraday efficiency of the Ni_2P-G@NF electrode was further measured in 0.5 M H_2SO_4 and it is about ~100% under an overpotential of 277 mV (Figure S6).

We further examined the stability of the Ni_2P-G@NF electrode for HER in 0.5 M H_2SO_4. After continuous CV scans for 300 and 500 cycles at a scan rate of 5 mV/s from 0 V to -0.20 V vs. RHE (Figure 3c), the curves showed negligible degradation even after 500 cycles. The stability of the electrode was also studied in 0.5 M H_2SO_4 by bulk electrolysis with an applied overpotential of ~55 mV to obtain the current density of 10 mA/cm^2 (Figure 3d). Importantly, there was no significant decrease of the catalytic current density after 15 hours.

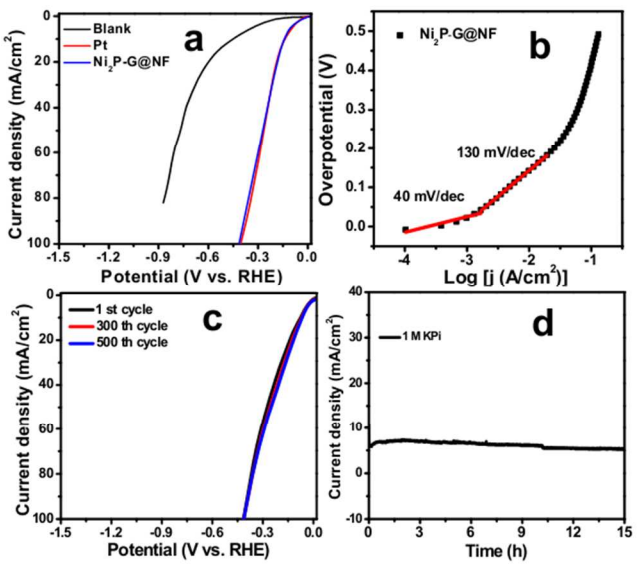

Figure 4. a) Polarization curves of Ni_2P-G@NF electrode in 1 M KPi (pH = 7) with a scan rate of 5 mV s^{-1}, along with G@NF and a Pt electrode for comparisions; b) The Tafel plot for the Ni_2P-G@NF electrode obtained from the polarization; c) Polarization data for the Ni_2P-G@NF electrode in 1 M KPi initially and after 300, 500 CV sweeps; d) Time-dependent current density for Ni_2P-G@NF electrode under over potential of 50 mV for 15 h.

Metallic Ni is not quite stable in strong acid, which may affect the catalytic performance for HER under acidic conditions. Therefore, we prepared a Ni_2P@G cathode by removing Ni and used it for HER in 0.5 M H_2SO_4 (Figure S7). The linear sweep CV curve of Ni_2P@G electrode in 0.5 M H_2SO_4 showed comparable catalytic current density (a little bit lower) to Ni_2P-G@NF electrode (Figure S7a). The result shows that the graphene layers could support the Ni_2P catalyst and help transfer electrons during catalysis. The slope based on the Tafel plot was found to be 38 mV/dec, indicating a good catalytic activity of the Ni_2P@G cathode (Figure S7b). It is proposed that the desorption process (Heyrovsky reaction) is the rate-determining step in which the expected slope was 40 mV per decade.[32] The high stability was observed by CV scans after 500 cycles (Figure S7c) and by the chronopotentiometry method with an applied overpotential of ~100 mV to obtain the current density of 8 mA/cm^2 for 24 hours (Figure S7d). The Faraday efficiency of Ni_2P@G cathode was measured in strong acid and it achieves a value of ~100% under an overpotential of 277 mV (Figure S8).

The Ni_2P-G@NF cathode is also an active HER catalyst under neutral conditions, as illustrated in Figure 4. The polarization curve of the Ni_2P-G@NF electrode in a 1.0 M Pi solution is shown in Figure 4a. The onset potential for HER is surprisingly low, being almost the same as Pt at the starting point, and then performs similar current density compared to Pt after an overpotential of only 15 mV. The rapid increase of catalytic current density is accompanied by vigorous H_2 evolution around the electrode. The performance is much higher than CoP/CC and the CoS under the same conditions.[22,26] In contrast, the G@NF cathode containing no Ni_2P shows much lower activity than the Ni_2P-G@NF cathode under the same conditions, indicating the important role of Ni_2P. For instance, G@NF requires 300 mV higher overpotential than Ni_2P-G@NF to achieve the same current density at 10 mA/cm^2 (Figure 4a, red plot). To obtain a moderate current density at 5 mA/cm^2, the Ni_2P-G@NF cathode needs an overpotential of only 50 mV, while other heterogeneous catalysts made of earth-abundant materials typically require an overpotential of > 65 mV to obtain 2 mA/cm^2 (Table S2).

Importantly, the Ni_2P-G@NF electrode exhibits a Tafel slope of ~40 mV/dec in the region of 0 ~ 40 mV (Figure 4b), in which the desorption process (Heyrovsky reaction) was also the rate-determining step.[32] This value is lower than that of the reported HER catalysts performing under neutral conditions, such as CoS.[22] In a region with higher overpotentials between 40 and 160 mV, the slope of the Tafel plot increased to 130 mV/dec. The present results do not match any value of three principle steps for hydrogen evolution (29, 38, 116 mV/dec).[33] Specially, a Tafel slope of >120 mV/dec is generally associated with a proton-coupled electron transfer (PCET) mechanism and not a metal hydride-based mechanism which generally has a Tafel slope of <60 mV/dec.[36] However, they are comparable to the values measured for other HER catalysts, including CoP/CC (93 mV/dec), CoS film (93 mV/dec),[22], amorphous M-MoS_3 (M = Fe, Co, Ni) films (86-96 mV/dec),[14] and crystalline Cu_2MoS_4 (86-96 mV/dec).[37] Furthermore, the Ni_2P-G@NF electrode shows great stability after 500 CV scans (Figure 4c), as well as achieving stable current density (5 mA/cm^2 under an overpotential of only 50 mV, Figure 4d). All the results indicate that the Ni_2P-G@NF cathode is among the best noble-metal-free HER electrocatalysts under neutral conditions, as seen in Table S2. The Faraday efficiency is close to 100% using the Ni_2P-G@NF cathode under an overpotential of 277 mV (Figure S9).

In addition, the Ni_2P-G@NF cathode also exhibited very high activity and durability for HER performance under alkaline conditions. Figure 5a shows the polarization curve of the Ni_2P-G@NF electrode in 1 M KOH (pH ~14). The onset overpotential is as low as 7 mV, which is the lowest overpotential among the reported literatures in alkaline solutions (pH ~14). The Faraday efficiency of the Ni_2P-G@NF electrode is measured with an overpotential of 7 mV and there was obvious H_2 evolution under this conditions (Figure S10). For comparison, the G@NF electrode showed a much lower performance than the Ni_2P-G@NF electrode. To achieve the same current density of 20 mA/cm^2, the G@NF electrode requires 150 mV higher overpotential than the Ni_2P-G@NF electrode (Figure 5b). The Ni_2P-G@NF electrode has a Tafel slope as low as ~30 mV/dec in the region of 0~30 mV, which is lower than the CoP/CC electrode under the same conditions.[26] The rate limiting step could be the recombination reaction (Tafel reaction).[32] At high overpotentials (η = 30-130 mV), the Tafel slope was increased to ~110 mV/decade. Similar to the results obtained at pH ~0, the value also does not match well with the expected Tafel slopes of 29, 38, and 116 mV/decade, each of which correlates with a different rate-determining step of the HER.[33] To achieve the catalytic current density of 10 mA/cm^2 for HER requires an overpotential of only ~50 mV (Figure 5a), which is better than many noble-metal-free HER catalysts, as seen in Table S3. The Ni_2P-G@NF electrode also showed a Faraday efficiency close to 100% for HER, with good stability and durability under alkaline conditions (Figure S11, and Figures 5c and 5d). We have made additional experiments to check the stability of the 3D Ni_2P-G@NF in the presence of CO saturated alkaline solutions, as seen in Figure S12. The LSV curve was nearly the same the presence of CO as that in the air saturated solution (Figure S12). The catalyst activity of 3D Ni_2P-G@NF was almost unaffected by CO while CO is known as an inhibitor of Pt because CO can bind to the electron-rich Pt (0) surface. These results were in consistent with the reported molybdenum or tungsten-based HER catalysts.[36,38-39]

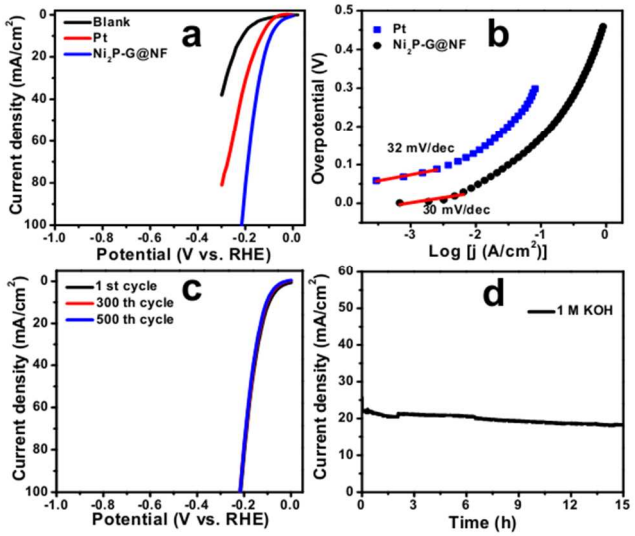

Figure 5. a) Polarization curves of Ni_2P-G@NF electrode in 1 M KOH (pH ~14) with a scan rate of 5 mV s^{-1}, along with G@NF and a Pt electrode for comparison; b) The Tafel plot for the Ni_2P-G@NF electrode and the Pt electrode obtained from the polarization; c) Polarization data for the Ni_2P-G@NF electrode in 1 M KOH initially and after 300, 500 CV sweeps; d) Time-dependent current density for Ni_2P-G@NF electrode under overpotential of 50 mV for 15 h.

Three more experiments were conducted to further examine the stability of Ni_2P@G and Ni_2P-G@NF electrodes for HER performance. First, bulk electrolysis experiments were carried out in three different solutions. The potentials were switched between -0.07 V and -0.17 V in 0.5 M H_2SO_4 solution, between -0.05 V and -0.08 V in 1.0 M Pi solution, and between -0.08 V and -0.10 V (vs. RHE) in 1 M KOH solution. The experiments were repeated more than 10 cycles (> 5 hours). During the cycles, the current density remained fairly stable (Figure 6a-c). These results confirmed good stability of Ni_2P@G and Ni_2P-G@NF for HER from acidic solution to alkaline solution (pH 0-14). Second, the XRD patterns of Ni_2P-G@NF electrode remained similar to those before electrolysis in a 1 M KOH solution (Figure 6d). Third, the EDX spectrum of the Ni_2P@G electrode after electrolysis in a 0.5 M H_2SO_4 confirmed a 2:1 atomic rate of Ni and P, as seen in Figure S13.

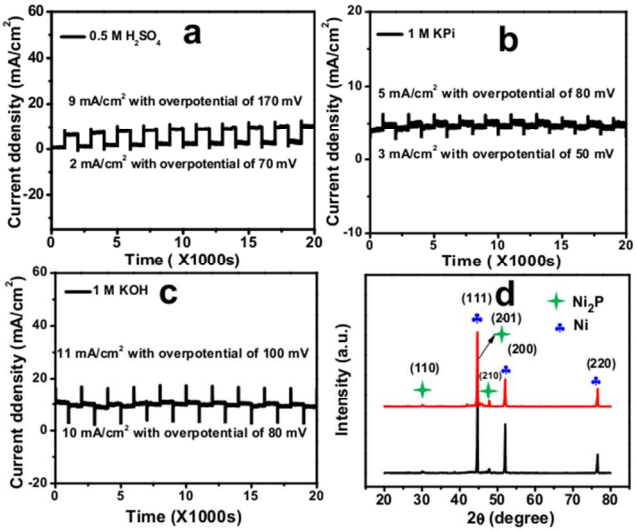

Figure 6. Time dependence of catalytic currents during electrolysis under different overpotentials in (a) 0.5 M H_2SO_4; (b) 1.0 M Pi; and (c) 1 M KOH after 10 cycles using Ni_2P@G, Ni_2P-G@NF, and Ni_2P-G@NF, respectively, as the working electrode; d) XRD patterns of the as-prepared 3D Ni_2P-G@NF electrode before (black) and after electrolysis (red) in 1 M KOH for 15 h.

Such high catalytic performance for HER using Ni_2P-G@NF cathode can be explained as follows: (1) more catalytically-active sites are provided due to the larger surface area of the G@NF (20 cm^2 per nominal area, which is ~20 times larger than that of a flat current collector[28]), which facilitates high performance HER reaction under the same applied cathodic potential. Besides, the catalytic activity of the 3D Ni_2P-G@NF for HER was normalized as a flat surface area, as seen in Figure S14; (2) the 3D framework structure provides a highly conductive network to effectively transfer electrons to the active material, allowing for fast transport of the electrolyte ions; (3) graphene sheets favor fast electron transfer through the electrode along the axial plane;[40] (4) direct growth of Ni_2P on G@NF allows robust mechanical adhesion without an external binder and facilitates interfacial

electron transfer between the catalysts and the electrodes, which can subsequently enhance the catalytic efficiency; (5) the 3D G@NF shows long-time stability and high conductivity in neutral and alkaline solutions. In addition, our system probably has the following disadvantages: (1) the Ni_2P-G@NF electrode is not very stable in acidic solution because the nickel substrate reacts with acid, which deactivate the catalytic activity of Ni_2P-G@NF; (2) Ni_2P material could be oxidized when it is exposed to air for long time; (3) The synthesis of Ni_2P requires red phosphorus, which react with nickel at a relatively high temperature (~750 ºC).

Conclusions

In summary, a 3D Ni_2P-G@NF electrode was successfully synthesized by direct growth of Ni_2P on G@NF *via* a simple heating reaction. All of the materials are inexpensive and earth-abundant. The resulting cathode shows a quite high activity in catalytic hydrogen production compared with nickel foam, CoP, bare Ni_2P, and even platinum. This good performance is due to a synergistic effect of 3D framework structure, the good contact between the conductive materials and the catalyst, graphene layers and highly active Ni_2P nanoflakes. The results indicate that 3D G@NF supported noble-metal-free catalysts are promising in applications for highly efficient water splitting, and potentially important for photocatalytic hydrogen production in the future.

This work was financially supported by the National Natural Science Foundation of China (21271166, 21473170), the Fundamental Research Funds for the Central Universities, the Program for New Century Excellent Talents in University (NCET).

Notes and references

CAS Key Laboratory of Materials for Energy Conversion, Department of Materials Science and Engineering, and the Collaborative Innovation Center of Chemistry for Energy Materials (iChEM), University of Science and Technology of China (USTC), Hefei, China 230026, Tel/Fax: 86-551-63606207; E-mail: dupingwu@ustc.edu.cn

† Electronic Supplementary Information (ESI) available: Experimental details, additional electrochemical data, XRD data and SEM images. See DOI: 10.1039/b000000x/

(1) Gray, H. B. *Nat. Chem.* **2009**, *1*, 7.
(2) Lewis, N. S.; Nocera, D. G. *Proc. Natl. Acad. Sci. U.S.A.* **2006**, *103*, 15729-15735.
(3) Armaroli, N.; Balzani, V. *Angew. Chem. Int. Ed.* **2006**, *46*, 52-66.
(4) Dresselhaus, M. S.; Thomas, I. L. *Nature* **2001**, *414*, 332-337.
(5) Walter, M. G.; Warren, E. L.; McKone, J. R.; Boettcher, S. W.; Mi, Q. X.; Santori, E. A.; Lewis, N. S. *Chem. Rev.* **2010**, *110*, 6446-6473.
(6) Cook, T. R.; Dogutan, D. K.; Reece, S. Y.; Surendranath, Y.; Teets, T. S.; Nocera, D. G. *Chem. Rev.* **2010**, *110*, 6474-6502.
(7) Du, P.; Eisenberg, R. *Energy Environ. Sci.* **2012**, *5*, 6012-6021.
(8) Eckenhoff, W. T.; McNamara, W. R.; Du, P.; Eisenberg, R. *Biochim. Biophys. Acta, Bioenerg.* **2013**, *1827*, 958-973.
(9) Esswein, A. J.; Nocera, D. G. *Chem. Rev.* **2007**, *107*, 4022-4047.
(10) Zheng, Y.; Jiao, Y.; Jaroniec, M.; Qiao, S. Z. *Angew. Chem., Int. Ed.* **2014**, online published. DOI: 10.1002/anie.201407031.
(11) Wang, M.; Sun, L. *ChemSusChem* **2010**, *3*, 551-554.
(12) Vrubel, H.; Merki, D.; Hu, X. L. *Energy Environ. Sci.* **2012**, *5*, 6136-6144.
(13) Voiry, D.; Yamaguchi, H.; Li, J. W.; Silva, R.; Alves, D. C. B.; Fujita, T.; Chen, M. W.; Asefa, T.; Shenoy, V. B.; Eda, G.; Chhowalla, M. *Nat. Mater.* **2013**, *12*, 850-855.
(14) Merki, D.; Vrubel, H.; Rovelli, L.; Fierro, S.; Hu, X. L. *Chem. Sci.* **2012**, *3*, 2515-2525.
(15) Liao, L.; Wang, S. N.; Xiao, J. J.; Bian, X. J.; Zhang, Y. H.; Scanlon, M. D.; Hu, X. L.; Tang, Y.; Liu, B. H.; Girault, H. H. *Energy Environ. Sci.* **2014**, *7*, 387-392.
(16) Raj, I. A.; Vasu, K. I. *J. Appl. Electrochem.* **1990**, *20*, 32-38.
(17) Brown, D. E.; Mahmood, M. N.; Man, M. C. M.; Turner, A. K. *Electrochim. Acta* **1984**, *29*, 1551-1556.
(18) Brown, D. E.; Mahmood, M. N.; Turner, A. K.; Hall, S. M.; Fogarty, P. O. *Int. J. Hydrogen Energy* **1982**, *7*, 405-410.
(19) Nocera, D. G. *Acc. Chem. Res.* **2012**, *45*, 767-776.
(20) Ahn, S. H.; Hwang, S. J.; Yoo, S. J.; Choi, I.; Kim, H. J.; Jang, J. H.; Nam, S. W.; Lim, T. H.; Lim, T.; Kim, S. K.; Kim, J. J. *J. Mater. Chem.* **2012**, *22*, 15153-15159.
(21) Chen, W. F.; Sasaki, K.; Ma, C.; Frenkel, A. I.; Marinkovic, N.; Muckerman, J. T.; Zhu, Y. M.; Adzic, R. R. *Angew. Chem. Int. Ed.* **2012**, *51*, 6131-6135.
(22) Sun, Y. J.; Liu, C.; Grauer, D. C.; Yano, J. K.; Long, J. R.; Yang, P. D.; Chang, C. J. *J. Am. Chem. Soc.* **2013**, *135*, 17699-17702.
(23) Chen, C.; Kang, Y. J.; Huo, Z. Y.; Zhu, Z. W.; Huang, W. Y.; Xin, H. L. L.; Snyder, J. D.; Li, D. G.; Herron, J. A.; Mavrikakis, M.; Chi, M. F.; More, K. L.; Li, Y. D.; Markovic, N. M.; Somorjai, G. A.; Yang, P. D.; Stamenkovic, V. R. *Science* **2014**, *343*, 1339-1343.
(24) Popczun, E. J.; McKone, J. R.; Read, C. G.; Biacchi, A. J.; Wiltrout, A. M.; Lewis, N. S.; Schaak, R. E. *J. Am. Chem. Soc.* **2013**, *135*, 9267-9270.
(25) Feng, L. G.; Vrubel, H.; Bensimon, M.; Hu, X. L. *Phys. Chem. Chem. Phys.* **2014**, *16*, 5917-5921.
(26) Tian, J. Q.; Liu, Q.; Asiri, A. M.; Sun, X. P. *J. Am. Chem. Soc.* **2014**, *136*, 7587-7590.
(27) Ji, J.; Zhang, L.; Ji, H.; Li, Y.; Zhao, X.; Bai, X.; Fan, X.; Zhang, F.; Ruoff, R. S. *ACS Nano* **2013**, *7*, 6237-6243.
(28) Ji, H.; Zhang, L.; Pettes, M. T.; Li, H.; Chen, S.; Shi, L.; Piner, R.; Ruoff, R. S. *Nano Lett.* **2012**, *12*, 2446-2451.
(29) An, C. H.; Wang, Y. J.; Wang, Y. P.; Liu, G.; Li, L.; Qiu, F. Y.; Xu, Y. A.; Jiao, L. F.; Yuan, H. T. *RSC Adv.* **2013**, *3*, 4628-4633.
(30) Zhang, S.; Zhang, S.; Song, L.; Wu, X.; Fang, S. *Mater. Res. Bull.* **2014**, *53*, 158-162.
(31) Popczun, E. J.; Read, C. G.; Roske, C. W.; Lewis, N. S.; Schaak, R. E. *Angew. Chem. Int. Ed.* **2014**, *53*, 5427-5430.
(32) Kucernak, A. R. J.; Sundaram, V. N. N. *J. Mater. Chem. A* **2014**, *2*, 17435-17445.

(33) Bockris, J. O. M.; Potter, E. C. *J. Electrochem. Soc.* **1952**, *99*, 169-186.
(34) Kibsgaard, J.; Chen, Z. B.; Reinecke, B. N.; Jaramillo, T. F. *Nat. Mater.* **2012**, *11*, 963-969.
(35) Lukowski, M. A.; Daniel, A. S.; Meng, F.; Forticaux, A.; Li, L. S.; Jin, S. *J. Am. Chem. Soc.* **2013**, *135*, 10274-10277.
(36) Chatterjee, S.; Sengupta, K.; Dey, S.; Dey, A. *Inorg. Chem.* **2013**, *52*, 14168-14177.
(37) Tran, P. D.; Nguyen, M.; Pramana, S. S.; Bhattacharjee, A.; Chiam, S. Y.; Fize, J.; Field, M. J.; Artero, V.; Wong, L. H.; Loo, J.; Barber, J. *Energy Environ. Sci.* **2012**, *5*, 8912-8916.
(38) Merki, D.; Hu, X. L. *Energy Environ. Sci.* **2011**, *4*, 3878-3888.
(39) Appel, A. M.; DuBois, D. L.; DuBois, M. R. *J. Am. Chem. Soc.* **2005**, *127*, 12717-12726.
(40) Wu, J. H.; Hagelberg, F. *Phys. Rev. B* **2007**, *76*, 155409.

TOC Figure:

A robust, highly efficient cathode containing three-dimensional Ni_2P/graphene/nickel foam has been successfully constructed for electrocatalytic H_2 evolution reaction (HER). The results show that 3D Ni_2P-G@NF cathode exhibits extraordinarily high activity for HER from pH 0-14.